Biomaterials 198 (2019) 27–36

Contents lists available at ScienceDirect

Biomaterials

journal homepage: www.elsevier.com/locate/biomaterials

Ex vivo synthetic immune tissues with T cell signals for differentiating antigen-specific, high affinity germinal center B cells

Alberto Purwada [a], Shivem B. Shah [a], Wendy Béguelin [b], Avery August [c], Ari M. Melnick [b], Ankur Singh [a, d, e, *]

[a] Meinig School of Biomedical Engineering, Cornell University, Ithaca, NY, 14853, USA
[b] Division of Hematology/Oncology, Department of Medicine, Weill Cornell Medicine, Cornell University, New York, NY, 10021, USA
[c] Department of Microbiology and Immunology, Cornell University, Ithaca, NY, 14853, USA
[d] Sibley School of Mechanical and Aerospace Engineering, Cornell University, Ithaca, NY, 14853, USA
[e] Englander Institute for Precision Medicine, Weill Cornell Medicine, New York, NY, 10021, USA

ARTICLE INFO

Article history:
Received 19 March 2018
Received in revised form
10 June 2018
Accepted 22 June 2018
Available online 26 June 2018

Keywords:
Infection
Immunity
Hydrogel
Tissue engineering
Integrin
Antibody

ABSTRACT

Most antigen discovery and vaccine development aimed at driving functional B cell responses rely on mouse immunizations studies. To date, there is no 3D *ex vivo* immune tissues, which are capable of driving antigen-specific B cell responses to rapidly determine the humoral immunogenicity of antigens, understand the role of extracellular matrix in humoral immunity, and generate high affinity antibody responses. This can be attributed to the complexity of B cell differentiation and affinity maturation process in the germinal center (GC) reaction, which makes these highly specialized cells susceptible to rapid apoptosis *ex vivo*. We have previously reported immune tissues that show *ex vivo* GC-like response, however in a non-antigen specific manner. Here, we report a maleimide (MAL)-functionalized polyethylene glycol (PEG)-based designer immune tissues that modulate B cell differentiation and enriches antigen-specific GC B cells in the presence of T-cell like signals. With the 3D synthetic immune tissue platform, we assessed various hydrogel design parameters to control *ex vivo* GC reaction. Using an $Ezh2^{fl/fl}$ Cγ1-cre transgenic mouse model, we demonstrated *ex vivo* IgG1 antibody class switching. Using immune tissues developed from a $B1\text{-}8^{hi}$ mutant mouse that represents a recombined antibody variable region derived from a 4-hydroxy-3-nitrophenylacetyl (NP) hapten binding antibody (B1-8), we demonstrate antigen specificity and selective enrichment of antigen-specific B cells with high affinity at both cell surface and secreted levels in integrin ligand-dependent manner. The *ex vivo* antigen-specific platform technology offers use in scientific understanding of immunobiology, matrix immunology, and in biotechnology applications, ranging from the antigen testing, vaccine development, and generation of antibodies against diseases.

© 2018 Elsevier Ltd. All rights reserved.

1. Introduction

Upon T cell-dependent activation, naïve B cells form germinal center (GCs) and undergo massive proliferation, somatic hypermutation, and affinity-based selection prior to differentiation into memory B cells [1–5]. Despite our deep understanding of immunity, it is difficult to study modulators of GC *in vivo* since natural GCs are heterogeneous and composed of B cells continuously recycling between dark and light zones of GCs. GC B cells with low expression of C-X-C Chemokine Receptor Type 4 (CXCR4) and high expression of CD83 surface marker are found in the less proliferative light zone of GCs, where the selection process occurs ahead of GC exit for terminal differentiation [4]. In contrast, GC B cells undergoing proliferation in the dark zone exhibit higher expression of CXCR4 surface marker and low expression of CD83 surface markers [4]. *In vivo*, B cell follicles are composed of a dense stromal network of B cell activating follicular dendritic cells (FDCs) [6,7], CD40 ligand (CD40L) presenting follicular T helper cells (T_{FH}), and extracellular matrix (ECM) such as Arg-Gly-Asp (RGD)-rich vitronectin [8]. B cell activation requires interaction between antigen-primed B cells and

* Corresponding author. 389 Kimball Hall, Cornell University, USA.
E-mail address: as2833@cornell.edu (A. Singh).

https://doi.org/10.1016/j.biomaterials.2018.06.034
0142-9612/© 2018 Elsevier Ltd. All rights reserved.

T_{FH} cells, which present CD40L and secrete interleukin (IL)-4, among others [7,10]. GC B cells also upregulate the expression of αvβ3 integrins, which binds to RGD-containing vitronectin protein [8,11]. In addition to vitronectin, another source of integrin signaling in GCs is the binding of α4β1 integrins on GC B cells to Vascular Cell Adhesion Molecule 1 (VCAM-1) on FDCs [8,12,13].

A major impediment to generating antigen-specific, high affinity, germinal center cells in a non-transgenic setting is the lack of simple experimental systems that sufficiently recapitulate the complex GC biology and allow for antigen specificity. Although it is possible to activate B cells *ex vivo*, the resulting proliferating and class switching B cells are more akin to the poor affinity non-GC extrafollicular response with distinct differences from *in vivo* GC B cells [5,14]. Therefore, there is an unmet need for an *ex vivo* technology capable of recapitulating selective complexity of GC reaction and induce antigen-specific humoral immunity. We recently reported a gelatin-based *ex vivo* 3D immune tissue that recapitulated selective cell-cell signaling aspects of the GC process and presented an RGD-rich niche [14–16]. The *ex vivo* tissue-derived GC B cells showed remarkable similarity to *in vivo* GC B cells from immunized mice in terms of the GC phenotype, transcriptome, induction of the GC master regulators B Cell CLL/Lymphoma 6 (BCL6) and the Enhancer of zeste homolog 2 (EZH2) histone methyltransferase, as well as activation-induced cytidine deaminase and somatic hypermutation [14]. Furthermore, the RGD-rich tissue recapitulated the GC-specific conditional deletion of EZH2 [14]. Using this tissue model we demonstrated that EZH2, which represses gene expression by catalyzing histone 3 lysine 27 trimethylation (H3K27me3), mediates GC formation through epigenetic silencing of the cell cycle checkpoint gene cyclin dependent kinase inhibitor 1A (CDKN1A) [14], enabling a positive transcriptional feedback loop. These studies, however, did not demonstrate antigen specificity, as noted in a recent review by Gosselin et al. [17], where T-cell signal becomes critical for selective enrichment. Here, we report a maleimide (MAL)-functionalized polyethylene glycol (PEG)-based designer immune tissues for regulating *ex vivo* GC B cell phenotype, including CXCR4 and CD83, B cell differentiation signaling, and selective enrichment of antigen-specific GC B cells using a first apoptosis signal (FAS)-based approach.

2. Materials and methods

2.1. Biomaterials and peptides

Four-arm PEG-MAL with 20 kDa molecular weight was obtained from Laysan Bio (Arab, AL) with >90% purity. Integrin αvβ3-binding RGD peptide (GRGDSPC, >90% purity), scrambled peptide (GRDGSPC, >90% purity) integrin α4β1-binding REDV peptide (GREDVGC, >90% purity), and matrix metalloproteinases (MMP)-9 degradable VPM peptide (GCRDVPMSMRGGDRCG, >90% purity) were obtained from AAPPTec (Louisville, KY). Integrin αvβ3 inhibitor Cilengitide (a cyclic RGD) was obtained from Selleck Chemicals.

2.2. Immune cells

For experiments involving wildtype (WT) B cells, spleens were harvested from female C57BL/6 mice (Stock #: 000664), aged 10–18 weeks from the Jackson Laboratory (Bar Harbor, ME). For experiments utilizing antigen-specific B cells, spleens were obtained from male B1-8^{hi} mice (Stock #: 007594), aged 10–12 weeks from the Jackson Laboratory. For experiments involving conditional *Ezh2* knockout(KO) mice, spleens were obtained from Cγ1-cre^{+} *Ezh2*$^{fl/fl}$ mice obtained from the Melnick Lab at Weill Cornell Medicine. These mice were generated by crossing *Ezh2*$^{fl/fl}$ mice with the transgenic Cγ1-cre strain and then crossing the resulting heterozygous *Ezh2*$^{fl/WT}$, as reported earlier by us [14]. Naïve B cells were isolated from splenocyte with EasySep Mouse B Cell Isolation Kit from Stem Cell Technologies (Vancouver, Canada). 40LB cells were obtained from Dr. Daisuke Kitamura, generated from NIH/3T3 fibroblasts genetically engineered to express CD40L and secrete BAFF, as previously described [18]. 40LB cells were cultured with high glucose Dulbecco's Modified Eagle Medium (DMEM) medium containing 10% FBS and 1% penicillin streptomycin (P/S) with all components obtained from Thermo Fisher Scientific (Waltham, MA). Prior to encapsulation in tissues, 40LB cells were mitotically inhibited through incubation in cell culture complete medium containing 0.01 mg/mL Mitomycin C (Sigma-Aldrich, MO503) at 37 °C for 55 min and were rinsed twice with 10 mL of phosphate-bufferedsaline (PBS) before the encapsulation. All animal procedures were approved by Cornell University's Institutional Animal Care and Use Committee or those established by the Weill Cornell Medical College of Cornell University.

2.3. Antibodies

Anti-mouse antibodies used for flow cytometry included anti-CD19 (eBioscience, PE-Cy7, eBio1D3), anti-GL7 (eBioscience, Alexa Fluor 488, GL-7), anti-BCL6 (eBioscience, PE, BCL-DWN), EZH2 (eBioscience, eFluor 660, AC22), anti-IRF4 (eBioscience, PE, 3E4), anti-CD83 (eBioscience, eFluor 660, Michel-17), anti-CXCR4 (eBioscience, Alexa Fluor 488, 2B11), anti-major histocompatibility complex (MHC) Class II (BD Pharmingen, I-A/I-E, PE, 2G9), anti-p-Btk (eBioscience, Tyr551, PE, M4G3LN), anti-p-Syk (eBioscience, Tyr348, APC, moch1ct), and anti-p-Erk1/2 (eBioscience, Thr202/Tyr204, PerCP-eFluor 710, MILAN8R). NP-specific GC-like B cells assessment was carried out with fluorophore-conjugated NP (PE, Biosearch Technologies) to target free NP-specific BCR and anti-mouse anti-NP antibody (Alexa Fluor 647, Novus Biologicals, B1-8) to target bound NP-specific B cell receptor (BCR). Anti-mouse antibodies used for CD40L blocking included anti-CD40L (eBioscience, Functional Grade Purified, MR1), anti-α4 (BioLegend, 9C10 (MFR4.B)) and anti-β1 (BioLegend, HMb1–1). Antibodies used for confocal microscopy included anti-mouse anti-integrin β3 (eBioscience, purified, armenian hamster, 2C9.G3), anti-mouse anti-CD19 (eBioscience, purified, Rat, eBio1D3), anti-immunoglobulin M (IgM) (Abcam, purified, Rabbit, II/41), anti-armenian secondary antibody (Abcam, Alexa Fluor 488, Goat), anti-rat secondary antibody (Abcam, Alexa Fluor 594, goat), and anti-rabbit secondary antibody (Thermo Fisher Scientific, Alexa Fluor 633, goat).

2.4. Soluble factors

Murine recombinant IL-4 was purchased from Peprotech (Rocky Hill, NJ). BCR activation was performed with anti-mouse anti-IgM antibody (eBioscience, II/41). Fas stimulation was achieved with anti-mouse anti-FAS antibody (BD Pharmingen, Jo2). NP antigen was introduced with soluble NP(17)-ovalbumin (OVA) (Biosearch Technologies, 17 NP-to-OVA conjugation/molar ratio). These soluble factors were mixed with cell culture medium and added into the tissue immediately following encapsulation.

2.5. Immune tissue fabrication

Synthetic immune tissues containing 7.5% PEG-MAL [19,20] were fabricated using PEG-MAL macromer, adhesive peptides, and crosslinkers. PEG-MAL macromers were initially functionalized with thiolated adhesive peptides RGD or REDV with 4:1 MAL-to-peptide molar ratio for 30 min at 37 °C. MMP-9 degradable VPM peptide and non-degradable dithiothreitol(DTT) crosslinkers were

combined at a 50:50 VPM-to-DTT molar ratio and 4:1.5 MAL-to-crosslinker molar ratio. All components were diluted using PBS^{++} solution with pH 7.4 and 1% 4-(2-hydroxyethyl)-1-piperazineethanesulfonicacid (HEPES). Naïve B cells and 40LB stromal cells were suspended in the crosslinker solution prior to cell encapsulation. After 5 μL of PEG-MAL macromer solution was placed in the middle of a well of a non-treated 96 well plate, 5 μL of cell-containing crosslinker solution was injected into the droplet and mixed by pipetting 5 times. Hydrogel droplets were prepared and cured for 15 min at 37 °C for complete crosslinking. Fresh RoswellPark Memorial Institute (RPMI 1640) medium supplemented with 10% fetal bovineserum (FBS), 1% P/S, and 10 ng/mL IL-4 was then added to each hydrogel-based immune tissue.

2.6. Flow cytometry analysis

Cells were harvested from the immune tissues after 4 days of culture with enzymatic degradation for 1 h using a 125 U/mL Collagenase Type 1 (Worthington Biochemical) dissolved in serum-free RPMI medium. Cells suspension was then filtered to remove gel debris using MultiScreen Mesh Filter Plates with 96 Well Receiver Plate (EMD Millipore). Cells were re-suspended in FACS buffer containing antibodies (1:500 dilution), incubated on ice in the dark for 45 min, and then re-suspended in FACS buffer. Intracellular marker staining was performed with one-step protocol for intracellular proteins using eBioscience Foxp3/Transcription Factor Staining Buffer Set. Phosphorylation signaling protein staining was performed with a two-step protocol using an eBioscience Intracellular Fixation and Permeabilization Buffer Set. FACS buffer was prepared using PBS^{++} containing 2% (v/v) FBS and 5 mM ethylenediaminetetraaceticacid (EDTA). Flow cytometry data was acquired using Accuri C6 Flow Cytometer (BD Biosciences) and analyzed with FlowJo software.

2.7. Confocal microscopy imaging

For imaging studies, synthetic hydrogel immune tissues were prepared as described above using uncoated glass-bottom (no. 1.5 coverslip and 20 mm glass diameter) 35 mm dish from MatTek Corporation (Ashland, MA). On day 4 post-encapsulation, the immune tissues were fixed with 4% paraformaldehyde, rinsed with PBS++, incubated with blocking buffer, stained with primary antibodies overnight, stained with secondary antibodies for 4 h, and then immediately imaged using Zeiss LSM 710 confocal microscope. Blocking buffer was prepared using PBS++ containing 20% goat serum. Staining was performed with flow buffer containing antibodies (1:500 dilution). Washing was done using PBS solution.

2.8. Antibody secretion from tissues

For antibody secretion, tissues, encapsulating 20,000 B cells and 40,000 40LB cells, were cultured for 6 days in media containing 10 ng/mL IL-4. After 6 days, supernatant media was collected and stored at −80 °C. To measure the amount of NP-OVA specific antibodies created by each tissue sample, 96-well plates (Corning™ Costar™ 9018) were first coated with 100 μL of 20 μ μg/mL NP-OVA solution for 24 h at 4 °C. Wells were washed twice with wash buffer (1× PBS, 0.05% Tween™ 20) prior to 1 h of blocking using PBS with 0.1% Tween™ 20 and 1% BSA. 100 μL of media dilutions ranging from 1:200 to 1:50 were added to the coated plates and incubated overnight. Plates were washed four times prior to incubation with detection antibody (horseradishperoxidase (HRP)-conjugated anti-mouse Ig (H + L) polyclonal antibody) for 1 h. After 4 additional washes, 1× TMB solution was added for 15 min prior to the addition of stop solution (eBioscience™ TMB Solution (1×), Catalogue Number: 00-4201-56). Intensity values at 450 nm and background values at 570 were then recorded using a plate reader.

2.9. Statistical analysis

Statistical analysis was performed using GraphPad Prism software (La Jolla, CA). Data is generally presented as Mean ± S.E.M with significance as defined in figure legends. Statistics involved unpaired student t-test or ANOVA as indicated in figure legends. All experiments were repeated multiple times and presented plots are representative of repeats.

3. Result and discussion

3.1. Designer immune tissues controlled ex vivo B cell differentiation and isotype class switching

The immune tissues were engineered using PEG-MAL macromers functionalized with thiolated integrin ligand peptides, consisting of VCAM-1-mimicking REDV or vitronectin-mimicking RGD peptides or scrambled peptide, at maximum adhesive saturation density (3 mM). Tissues were crosslinked with di-thiolated MMP-cleavable peptide crosslinker [19,21]. The immune tissues contained both primary murine naïve B cells and engineered 40LB stromal cells [15,18] that express CD40L on the surface and secrete B Cell Activating Factor (BAFF), thus mimicking selective signals of T_{FH} cells and FDCs, respectively (Fig. 1A). Within 4 days of culture, the immune tissues showed a closely packed presence of B cells on top of the 40LB cells (Fig. 1B and C). Under the same growth conditions, 2D co-culture showed a more sparse distribution of B cells (Fig. 1B). Integrin ligands did not have a major influence on the expression level of GC phenotype, GL7 protein, except that a higher 40LB density resulted in higher GL7 surface expression (Fig. 1D). To determine at which time point these biological interactions occurred *ex vivo*, we blocked CD40L and integrins. When 40LB cells were blocked with anti-CD40L antibody on day 2, it showed similar induction of GC phenotype to the no blocking conditions, and significantly higher than early (t = 0) blocking time (Fig. 1E). These results suggest that the initial CD40L and B cell contact was critical for the differentiation of naïve B cells into $GL7^+$ GC B cells, *ex vivo*. We next examined the temporal dependence of the number of GC B cells on integrin signaling by inhibiting αvβ3 integrin with Cilengitide and α4β1 stimulation using monoclonal antibodies. We observed a significant decrease in the number $GL7^+$ $CD19^+$ GC-like B cells when Cilengitide was added at t = 0 time point (Fig. 1F) in RGD hydrogels. But such effect was not seen with Cilengitide addition at later time points (t = 4 or 12 h). GC reaction is also modulated by FDC-mediated VCAM-1 that binds to α4β1 integrins on GC B cells [8]. Early blockade of α4β1-REDV (VCAM-1) interaction had no effect on the induction of $GL7^+CD19^+$ B cells, whereas inhibition at 4 and 12 h markedly reduced the percentages of $GL7^+CD19^+$ B cells (Fig. 1F). Therefore, VACM-I interaction appears to be important at later times for sustained *ex vivo* GC reaction.

In order to assess if *ex vivo* immune tissue size can influence the resulting phenotype, we determined the role of hydrogel volume on GC reaction. While we observed no significant differences in GL7 surface marker expression between 6 and 10 μL hydrogels (Supplementary Figs. S1) and 10 μL hydrogel volume induced both higher percentage of $CD83^+CD19^+$ B cells (Fig. 1G) and higher CD83 surface expression level in $CD83^+CD19^+$ B cells (Fig. 1H). Importantly, the ratio of $CD83^+$ to $CD83^-$ B cells was ~2-fold higher when differentiation was performed in 10 μL tissues as compared to 6 μL tissues (Fig. 1I), suggesting larger hydrogel volume promoted $CD83^+$ phenotype. We confirmed this observation with the expression of CXCR4 in 6 and 10 μL tissues and observed a decrease

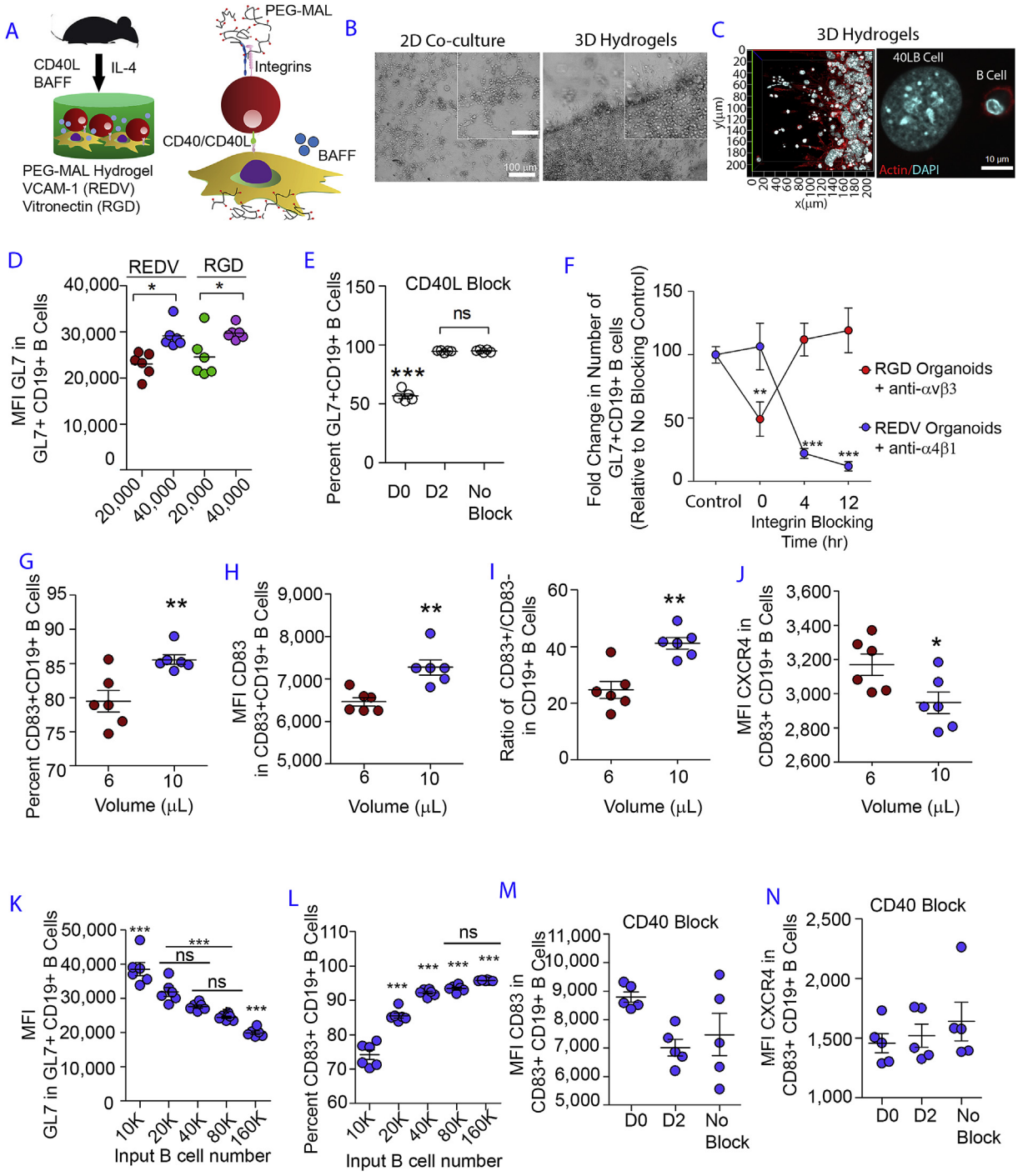

Fig. 1. Designer immune tissues control GC-like B cell phenotype. A) Schematic showing PEG-MAL hydrogels functionalized with REDV or RGD peptides and embedded with naïve B cells and 40LB stromal cells in the presence of soluble IL-4 cytokine. **B)** Phase contrast images show qualitative distribution of B cells in 2D co-cultures (left) and 3D immune tissues (right). **C)** Confocal images of 40LB stromal cells and B cells in 3D immune tissues. **D)** Role of integrin ligand and 40LB density on GC induction. Scatter plot represents median fluorescent intensity of GL7 in $GL7^{+}CD19^{+}$ GC B cells as a function of integrin ligand VCAM-1 (REDV) and vitronectin (RGD), and 40LB cell density (20,000 vs. 40,000 40LB cells per 10 μL hydrogel). N = 6; Mean ± S.E.M; $^{**}P < 0.005$, $^{*}P < 0.05$; 2-way ANOVA with Bonferroni correction. **E)** Effect of blocking CD40L on GC induction. Scatter plot represents percentage GL7+ $CD19^{+}$ GC-like B cells following culture in hydrogel functionalized with RGD in the presence of anti-CD40L antibody added at various time points in culture. N = 5; Mean ± S.E.M; $^{***}P < 0.0001$; 1-way ANOVA with Tukey's post-hoc correction. **F)** Temporal dependency of integrin−ligand interaction on GC B cells. Relative percentages of cells were quantified for $GL7^{+}$ $CD19^{+}$ GC-like B cells following culture in hydrogel functionalized with either REDV (blue) or RGD (red) in the presence of anti-α4β1 antibody or Cilengitide anti-αvβ3 peptide) added at various time points in culture. $GL7^{+}$ $CD19^{+}$ percentage was normalized to the no inhibitor treatment. N = 6; Mean ± S.E.M; Statistical significance was tested based on $p < 0.05$ using 2-way ANOVA with Bonferroni correction. $^{***}P < 0.0001$, $^{**}P < 0.001$. Control: No inhibitor. **G)** The percentage of $CD83^{+}$ $CD19^{+}$ B cells as a function of hydrogel volume. Immune tissues, encapsulating 40,000 B cells and 40,000 40LB cells, were cultured for 4 days in media containing 10 ng/mL IL-4. **H)** CD83 surface expression level in $CD83^{+}$ $CD19^{+}$ GC B cells as a function of hydrogel volume, cultured for 4 days. **I)** $CD83^{+}$ $CD19^{+}$ and $CD83^{-}$ $CD19^{+}$ B cells as a function of hydrogel volume, cultured for 4 days. **J)** CXCR4 surface expression level in $CD83^{+}$ $CD19^{+}$ GC B cells as a function of hydrogel volume, cultured for 4 days. **K-L)** GL7 expression in GL7+ $CD19^{+}$ GC-like B cell population and the percentage of $CD83^{+}$ $CD19^{+}$ GC B as a function of B cell seeding density in 10 μL PEG-MAL hydrogel, cultured for 4 days. $^{***}P < 0.0001$, $^{**}P < 0.001$, $^{*}P < 0.05$; 1 Way ANOVA with Tukey's Test. Values are shown as mean ± SEM (n = 5). **M-N)** CD83 and CXCR4 expression level based on median fluorescence intensity (MFI) in $CD83^{+}$ $CD19^{+}$ B cell population following 4-day culture in RGD hydrogel with the addition of anti-CD40L antibody to block CD40 signaling at day 0 (D0) and day 2 (D2). Control group was prepared with no blocking performed (No Block). Statistical significance was tested based on $p < 0.05$ using 1-way ANOVA with Tukey's test (N = 5; Mean ± S.E.M). (For interpretation of the references to color in this figure legend, the reader is referred to the Web version of this article.)

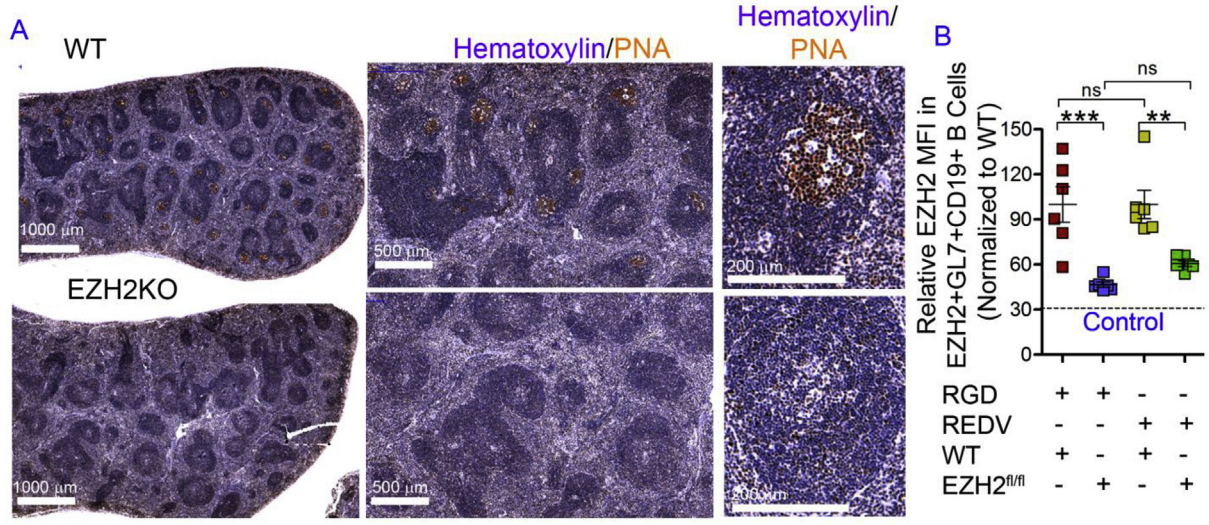

Fig. 2. Designer immune tissues facilitate isotype class switching. A) Formalin fixed paraffin embedded splenic tissue from immunized WT and *Ezh2*$^{fl/fl}$ Cγ1-cre (EZH2 KO) mouse stained for GC marker peanut agglutinin (PNA, brown) and hematoxylin (blue). One representative picture of three spleens analyzed is shown. **B)** The relative EZH2 MFI in EZH2+GL7+ CD19^{+} B cells derived in immune tissues using *Ezh2*$^{fl/fl}$ Cγ1-cre mouse derived naïve B cells and normalized to WT samples. Experiments were done with n = 6, presented as mean ± standard error (scatter plot only) with statistical significance indicated by $p < 0.05$ (***$P < 0.0001$, **$P < 0.001$). Statistical tests were performed using 1-way ANOVA with Tukey's correction. (For interpretation of the references to color in this figure legend, the reader is referred to the Web version of this article.)

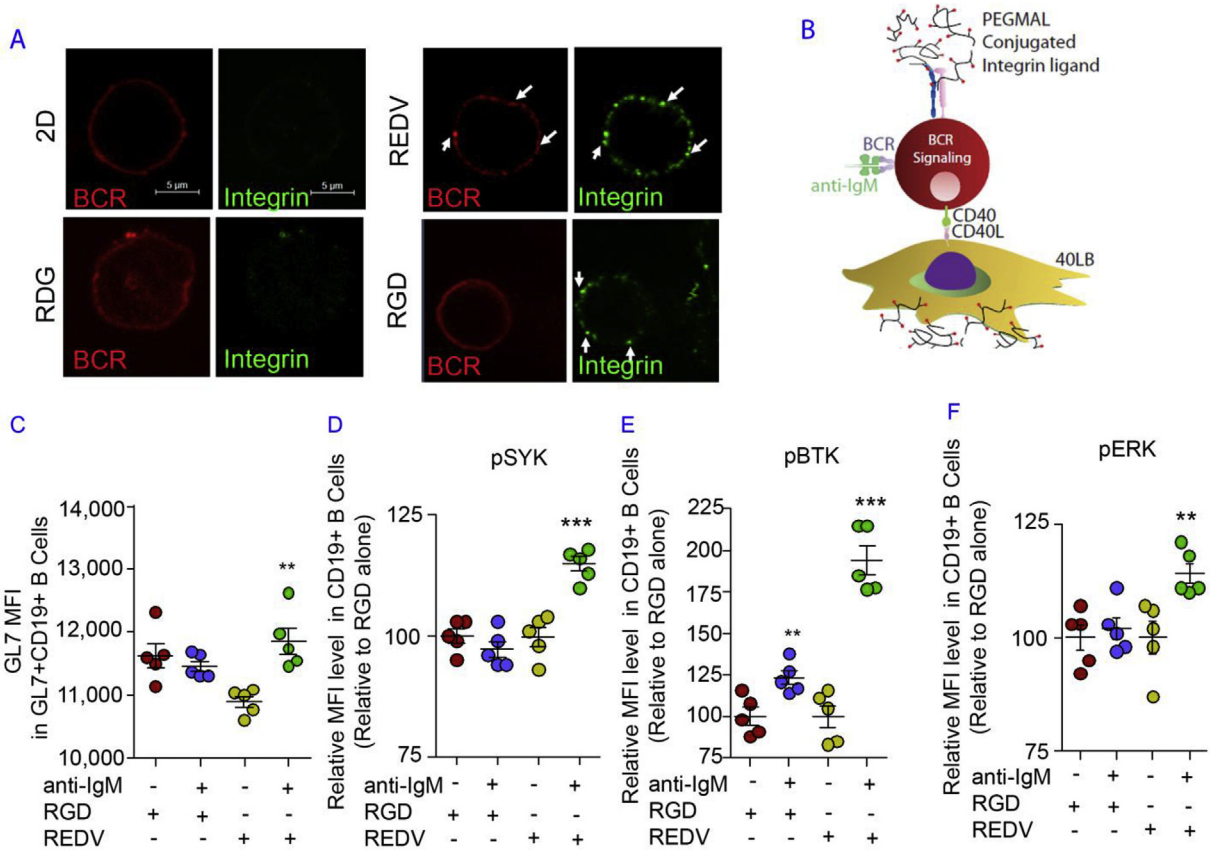

Fig. 3. Integrin ligands and BCR crosslinking in immune tissues modulate signaling proteins in B cell differentiation. A) Confocal images of day 4 B cells from 2D co-cultures or 3D immune tissues functionalized with a specific peptide (REDV, RGD, or RDG). Cells were stained for IgM BCR and integrin β subunits on the surface of CD19^{+} B cells. Scale bar 5 μm. In all studies, immune tissues, encapsulating 40,000 B cells and 40,000 40LB cells, were cultured for 4 days in media containing 10 ng/mL IL-4. **B)** Schematic showing the BCR crosslinking inside the immune tissues with anti-IgM antibody as an antigen mimic. **C)** GL7 surface expression level in GL7+ CD19^{+} GC-like B cells with/without BCR crosslinking and specific integrin ligands. **D-F)** pBTK, pSYK, and pERK intracellular expression level (normalized to untreated control group in RGD) in CD19^{+} B cells. In all studies, anti-IgM concentration was either 0 μ μg/mL (indicated as -) or 5 μ μg/mL (indicated as +). Experiments were done with n = 5–7, presented as mean ± standard error (scatter plot only) with statistical significance indicated by $p < 0.05$ (***$P < 0.0001$, **$P < 0.001$). Statistical tests were performed using 1-way ANOVA with Tukey's correction.

in the expression level of CXCR4 in CD83$^+$ CD19$^+$ B cells in 10 μL tissues (Fig. 1J; $p < 0.001$), which is consistent with the light zone phenotype. Although the goal of this study was not to show zonal patterning or migration between sections of immune tissues, as one sees *in vivo* in B cell follicles, our study, to the best of our knowledge, is the first evidence of controlled modulation of CD83 and CXCR4 expressing cells as a function of *ex vivo* tissue parameters. We observed decreasing GL7 expression level with higher naïve B cell density and this outcome could potentially be attributed to the lower amount of CD40L received by individual naïve B cells in the 3D tissue (Fig. 1K). We finally determined the role of naïve B cell seeding density in 10 μL tissues and observed an increased percentage of CD19$^+$ B cells that express CD83 surface marker with higher naïve B cell seeding density (Fig. 1L). Nevertheless, at 20,000 naïve B cell density, approximately 85% CD83$^+$CD19$^+$ B cells were formed and the GL7 expression levels were markedly high. Next, blocking of CD40L did not affect CD83 or CXCR4 expression levels suggesting that *ex vivo* expression of these phenotypic markers are independent of CD40L presentation (Fig. 1M and N, respectively).

In order to verify whether class switching into immunoglobulin G1 (IgG1) isotype occurred in the immune tissues, we utilized a *Ezh2*$^{fl/fl}$ Cγ1-cre transgenic mouse model. We have previously used the *Ezh2*$^{fl/fl}$ Cγ1-cre mouse model to show that EZH2 is required for GC reaction [22]. The effect of EZH2 in the GC reaction is not related to global H3K27 trimethylation. Instead, the specific role of EZH2 in GC B cells is to induce the de novo GC B cell specific formation of bivalent (H3K27me3 + H3K4me3) chromatin and hence transcriptional repression at a specific set of approximately 1000 gene promoters that EZH2 (but not EZH1) represses in the context of the GC B-cell [14,22–24]. In *Ezh2*$^{fl/fl}$ Cγ1-cre mouse, *Ezh2* excision occurs following the expression of Cre recombinase specifically within GC B cells and not just any B cells. When naïve CD19$^+$ B cells from *Ezh2*$^{fl/fl}$ Cγ1-cre mouse were seeded into the synthetic immune tissues, we observed a significant decrease in EZH2 expression in EZH2+ GL7+ GC-like B cells in the *Ezh2*$^{fl/fl}$ Cγ1-cre group as compared to the WT group (Fig. 2A and B). The percent drop in expression level was close to the isotype negative control, in both RGD and REDV functionalized tissues. However, such decrease in EZH2 expression was only evident with 40,000 CD40L-presenting stromal cells (Fig. 2B) but not at 20,000 40LB cell seeding density (Supplementary Fig. S2). This observation suggested the

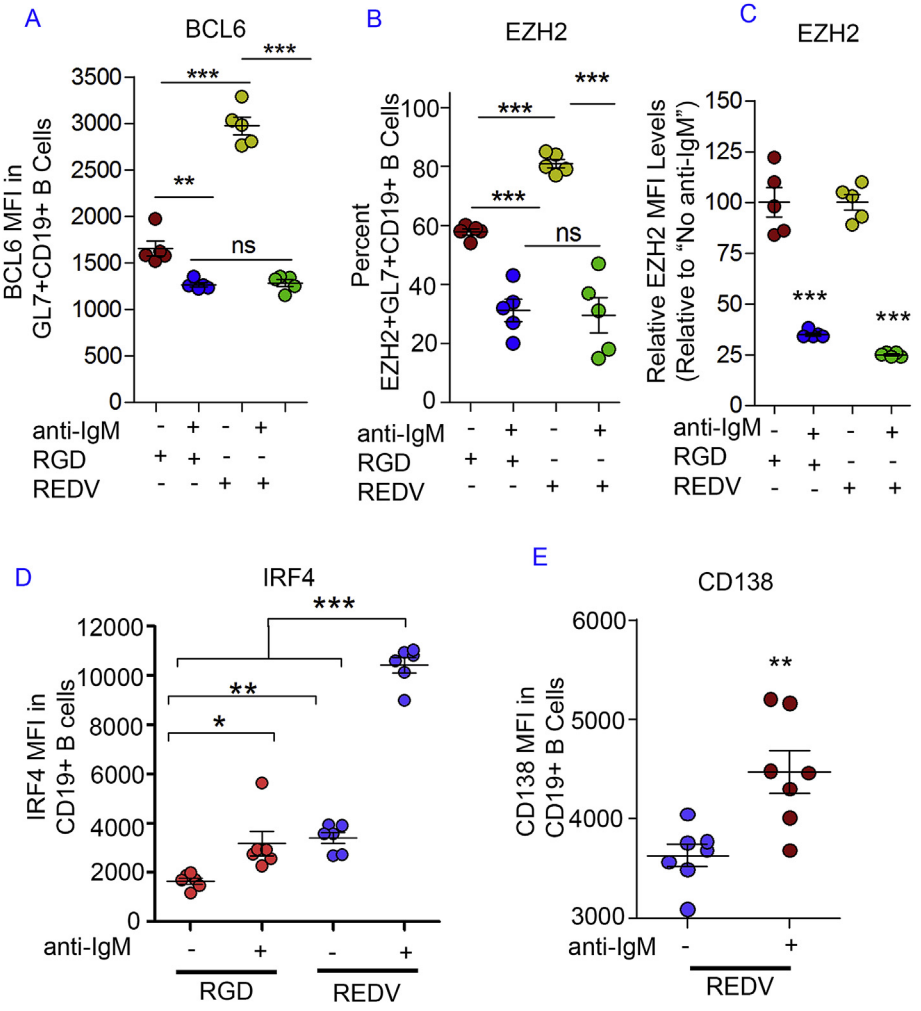

Fig. 4. Integrin ligands and BCR crosslinking in immune tissues modulate transcriptional regulators of B cell differentiation. A) BCL6 intracellular expression level in GL7$^+$ CD19$^+$ GC-like B cells with or without BCR crosslinking and specific integrin ligands. **B)** The percentage of EZH2$^+$ GL7$^+$ CD19$^+$ GC-like B cells with or without BCR crosslinking and specific integrin ligands. **C)** EZH2 intracellular expression level (normalized to untreated control group) in EZH2$^+$ GL7$^+$ CD19$^+$ GC-like B cells with or without BCR crosslinking and specific integrin ligands. **D-E)** IRF4 intracellular expression level and CD138 expression level in immune tissue-derived B cells. In all studies, anti-IgM concentration was either 0 μg/mL (indicated as -) or 5 μg/mL (indicated as +). Experiments were done with N = 5–7, presented as Mean ± Standard Error (scatter plot only) with statistical significance indicated by $p < 0.05$ (***P < 0.0001, **P < 0.001, *P < 0.05). Statistical tests were performed using unpaired student t-test for (E) and 1-way ANOVA with Tukey's correction for (A–D).

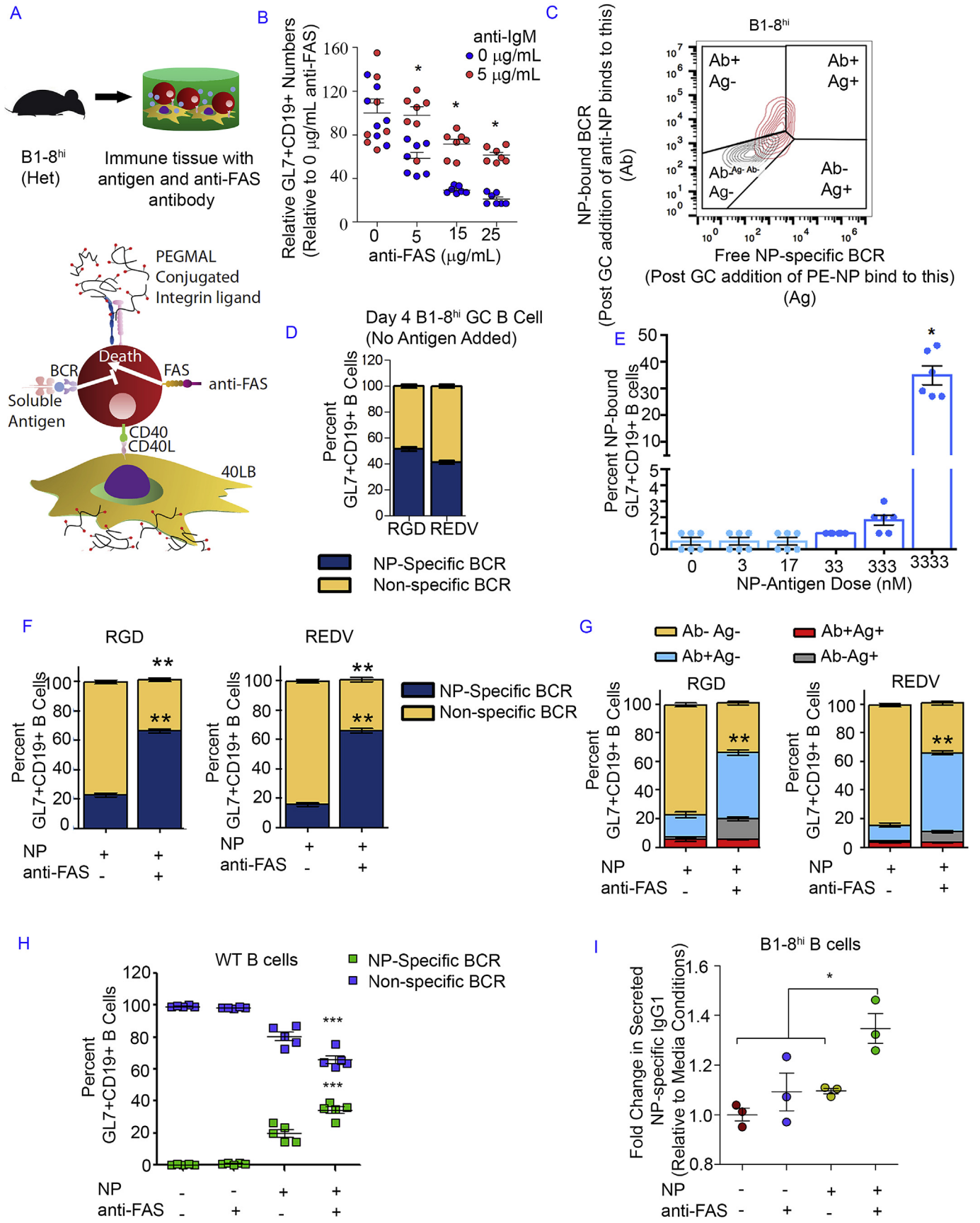

Fig. 5. Integrin ligands, BCR crosslinking, and FAS stimulation facilitated the enrichment of antigen-specific GC-like B cells. A) Schematic showing the enrichment methodology inside the immune tissues via CD40L-presenting 40LB stromal cells, soluble NP antigen or antigen mimic with anti-IgM antibody, and anti-FAS antibody. **B**) The change in

importance of high CD40L density to enable *ex vivo* class switching reaction in the presence of IL-4. Based on these observations, we performed our subsequent studies with 20,000 naïve B cells and 40,000 40LB stromal cells encapsulated using 10 μL hydrogel. As we have previously shown that whole GC transcriptome and somatic hypermutation in RGD rich hydrogels are comparable to *in vivo* immunized mice [14], these studies were not repeated here.

3.2. Integrin ligands and BCR crosslinking in immune tissues modulated signaling proteins and transcriptional regulators of B cell differentiation

B cell terminal differentiation is dependent on BCR signaling [2], which occurs with the binding of antigen by its corresponding BCR. The importance of α4β1-REDV (VCAM-1) interaction was evident in confocal studies, whereby GC B cells showed aggregated IgM B cell receptors, which co-localized with β subunit integrin (Fig. 3A). αvβ3-RGD interaction did not show aggregation of IgM BCR, whereas 2D and scrambled peptide RDG did not show clustered integrins on the surface of individual B cells in immune tissues. In both RDG scrambled peptide and 2D co-culture control groups, IgM B cell receptor was found to be mostly diffused throughout the outer surface. These results demonstrate that the hydrogel-mediated response is indeed dependent on bio-adhesive peptide ligands.

We hypothesized that crosslinking BCR with exogenous antigen mimic (anti-IgM antibody; Fig. 3B) will modulate GC differentiation in an integrin ligand-dependent manner. To test this hypothesis, $CD19^+$ naïve B cells were cultured with increasing concentration of 0–5 μg/mL of soluble anti-IgM antibody (an antigen mimic to crosslink BCR). The GL7 expression level in $GL7^+$ $CD19^+$ B cells (Fig. 3C) and CD83 expression level in $CD83^+$ $CD19^+$ B cells was markedly increased at 5 μg/mL anti-IgM dose as compared to lower doses (Supplementary Fig. S3) and to a slightly higher level in RGD tissues than REDV (VCAM-1) tissues (Supplementary Fig. S4). Our data also showed a significant 40% increase in MHCII expression, which is induced upon BCR activation, with 5 μg/mL anti-IgM antibody dose, therefore suggesting that multiple GC activation markers are induced with BCR activation (Supplementary Fig. S5).

We determined if the BCR crosslinking effects led to the phosphorylation of BCR target proteins in the immune tissues and whether such processes were dependent on the integrin ligand specificity. Upon antigen binding, SRC family kinases are known to get activated quickly prior to the phosphorylation of both SYK and BTK [25]. ERK phosphorylation occurs downstream of SYK activation [26] and therefore can be induced following BCR stimulation [27]. Our results showed a significant increase in the expression level of phosphorylated pSYK, pBTK, and pERK1/2 in REDV hydrogels with 5 μg/mL soluble anti-IgM antibody (Fig. 3D–F). Analysis of the normalized expression level indicated that pBTK expression increased by nearly 100% after BCR stimulation in REDV functionalized immune tissues, as compared to only 25% in RGD immune tissues (Fig. 3E). The levels of phosphorylated SYK (Fig. 3D) and ERK1/2 (Fig. 3F) also significantly increased following BCR stimulation in REDV group, but not in RGD immune tissues. These observations suggested BCR signaling was more sustained in REDV group when contrasted to that in RGD group.

We then assessed whether BCR crosslinking reduced the expression level of intracellular markers that are known to play a crucial role in GC reaction such as BCL6 and EZH2. BCL6 transcription factor regulates GC B cell development primarily by suppressing the transcription of plasma cell differentiation genes and this marker is only expressed in GC B cells [28]. The importance of BCL6 towards GC reaction is further supported by the lack of GC formation in BCL6-deficient mice [29]. Since BCR stimulation targets BCL6 and causes rapid degradation of this transcription factor [30], we hypothesized that anti-IgM mediated crosslinking will lower BCL6 expression. At 0 or 0.5 μg/mL anti-IgM dose, the BCL6 intracellular expression level was higher in REDV hydrogels when compared to the RGD hydrogels (Fig. 4A, Supplementary Fig. S6). In contrast, at 5 μg/mL dose, BCL6 expression was markedly lowered to the same level in both hydrogel types. Compared to the 0 μg/mL dose group, a greater reduction in BCL6 level was observed in REDV (VCAM-1) tissues. These observations suggest that REDV (VCAM-1)-functionalized immune tissues result in greater BCL6 induction during *ex vivo* GC reaction and increased responsiveness toward BCR stimulation, possibly towards a GC exit.

In addition to the GC transcription factor BCL6, a key epigenetic biomarker is EZH2. EZH2 is specifically expressed in GC B cells and primarily works by epigenetically silencing a set of differentiation genes [14,22]. EZH2 is critical for the GC reaction because *Ezh2* knock-out mice do not form GCs [14,22,24]. As shown in Fig. 4B and C, and Supplementary Fig. S7, we observed a significant reduction in the percentage of $EZH2^+$ GC-like B cells and a significant 70–75% reduction in EZH2 expression in $EZH2^+$ $GL7^+$ $CD19^+$ B cells after BCR stimulation with 5.0 μg/mL anti-IgM antibody dose as compared to lower doses. Without BCR stimulation, a greater EZH2+ population was also seen in REDV (VCAM-1) group than RGD group, likely because of matrix-mediated BCR crosslinking. While the percentage of $EZH2^+$ $GL7^+$ $CD19^+$ cells was similar at 5 μg/mL dose across integrin ligand types, a greater drop occurred in REDV (VCAM-1)-functionalized tissues when compared to that in the RGD-functionalized tissues.

We hypothesized that decreased GC marker is associated with increased plasma cell marker, which is indicative of the GC exit or terminal differentiation process. We observed an increase in the expression of plasma cell differentiation transcription factor **Interferon** regulatory factor 4 (IRF4), following the addition of soluble anti-IgM antibody into the synthetic immune tissues (Fig. 4D). IRF4 is a transcription factor that regulates GC B cell terminal differentiation and suppresses BCL6 [28]. We observed a statistically significant increase in IRF4 level at 5 μg/mL in RGD tissues. A greater IRF4 expression was seen at each dose in REDV tissues when compared to the corresponding anti-IgM dose in RGD tissues (average median fluorescence intensity (MFI) 10,400 in REDV versus 3100 in RGD with 5 μg/mL dose). These observations suggested that while BCR crosslinking facilitates IRF4 induction in both REDV and RGD immune tissues, a greater responsiveness

GL7+ $CD19^+$ GC-like B cell number (normalized to 0 μ μg/mL anti-FAS dose group) in the absence or presence of anti-IgM antibody and increasing anti-FAS antibody doses. Immune tissues, encapsulating 40,000 B cells and 40,000 40LB cells, were cultured for 4 days in media containing 10 ng/mL IL-4. **C**) Gating schematic indicating GC-like B cell segmentation based on the presence of free antigen receptor (Ag+) and/or bound antigen receptor (Ab+). **D**) The percentage of GC-like B cells with NP-specific and non-specific BCR following tissue culture with NP-specific primary B cells and no soluble NP antigen added. **E**) The percentage of NP-bound GC-like B cells following tissue culture with NP-specific primary B cells and an increasing dose of soluble NP antigen added to the cell culture media. **F**) The percentage of GC-like B cells with NP-specific and non-specific BCR following tissue culture with NP-antigen only or in combination with anti-FAS antibody. **G**) The detailed composition of GC-like B cells based on the availability of free antigen receptor (Ag+) and/or bound antigen receptor (Ab+) after tissue culture with NP-antigen only or in conjunction with anti-FAS antibody. **H**) The percentage of GC B cells from WT B cells in the presence of NP antigen and/or anti-FAS antibody in REDV tissues. **I**) The fold change in secreted NP-specific IgG1 levels in cell culture serum (n = 3). Immune tissues were cultured for 6 days in media containing 10 ng/mL IL-4. Experiments were done with n = 5–7, presented as mean ± standard error (bar graph or scatter plot only) with statistical significance indicated by $p < 0.05$ (***P < 0.0001, **P < 0.001, *P < 0.05). Statistical tests were performed using 1-way ANOVA with Tukey's correction for (D-F, G, I) and 2-way ANOVA with Bonferroni's correction for (B, H).

toward BCR stimulation was seen in REDV group. Finally, we also investigated CD138 expression, a marker of terminally differentiated B cells, and observed a significantly increased expression of CD138 in CD19$^+$ B cells following 5 μg/mL anti-IgM antibody additions (Fig. 4E). These trends suggested that BCR stimulation indeed facilitates the terminal differentiation program in B cells.

3.3. FAS stimulation facilitated the enrichment of antigen-specific GC-like B cells

After demonstrating the ability to modulate GC activation, we next determined whether tissues could generate antigen-specific GC B cells and induce selective enrichment of high affinity B cells. GC B cells can be enriched based on their affinity towards an antigen or by depleting non-specific cells through FAS-mediated apoptosis. Higher-affinity B cell clones bind more antigen, thereby crosslinking more BCR [31]. B cells with crosslinked BCR can survive apoptotic signal from FAS ligand presented by follicular helper T cells, leading to selective enrichment process [32]. In contrast, when activated B cells no longer receive a BCR signal, they are killed by FAS ligand expressed on activated T cells. We hypothesized that in an *ex vivo* system, crosslinking FAS on GC B cells may meet this requirement (Fig. 5A). We first tested our hypothesis by using a FAS ligand mimic (anti-FAS antibody to crosslink FAS) and an antigen mimic (IgM antibody to crosslink BCR like an antigen). Indeed, the addition of soluble anti-FAS antibody reduced the number of CD19$^+$ B cells and the rapid apoptosis was abrogated by anti-IgM antibody (Fig. 5B).

We further hypothesized that the FAS-mediated selection approach could be applied to selectively enrich a particular GC B cell clone with protein antigen-bound GC B cells being resistant toward FAS-induced apoptosis. In order to test this concept, we used the B1-8^{hi} mouse model to obtain primary B cells containing a high number of 4-Hydroxy-3-nitrophenyl (NP) acetyl-hapten-specific B cells. In the B1-8^{hi} mouse model, pre-recombined V_HDJ_H genes are incorporated into the mouse immunoglobulin heavy chain locus [33] and the resulting B1-8 heavy chain can bind NP upon pairing with the Igλ light chain [34]. An additional mutation of Trp to Leu introduced at codon 33 of the B1-8 heavy chain increases the NP binding affinity by a factor of 40 [33]. We simply added soluble NP antigen to the tissue culture and developed a flow cytometry gating schematic to separate non-specific and NP-specific GC-like B cells for the enrichment study. First fluorophore-conjugated antibody against NP was added to the tissue cultures after 4 days, followed by staining with NP conjugated to another color fluorophore (Fig. 5C). Such approach enabled us to identify NP-specific B cells with free BCR and/or NP-bound BCR. In the absence of antigen, the immune tissues with B1-8^{hi} cells from heterozygous mice generated equivalent % of GC like B cells with NP$^+$ free BCR (Fig. 5D). Since the enrichment process will require NP-specific B cells to undergo BCR crosslinking with the binding between NP and NP-specific BCR, we next examined the soluble NP antigen dose required to obtain a high number of NP-bound GC-like B cells and observed that a reasonable amount (~40%) of NP-bound GC-like B cells could be achieved with 3332 nM soluble NP antigen dose (Fig. 5E).

With the same soluble NP antigen dose, we then performed the selective enrichment process with FAS stimulation using 5 μg/mL anti-FAS antibody. The FAS stimulation significantly decreased the percentage of non-specific GL7$^+$ CD19$^+$ GC-like B cells and increased the percentage of NP-specific GL7$^+$ CD19$^+$ GC-like B cells (Fig. 5F). The final NP-specific GC-like B cell percentage was similar in both peptide groups following soluble NP antigen presentation and FAS stimulation, likely attributable to the dose of antigen. However, further analysis of the post-enrichment cells suggested a greater difference in the composition of GC-like B cell population in REDV group when compared to that in RGD group (Fig. 5G). Specifically, a higher percentage of fully bound GC-like B cells was found in REDV-functionalized immune tissues (a 55% increase relative to untreated control) when compared to the RGD group (a 46% increase relative to untreated control). This trend was followed by a greater percentage of partially bound GC-like B cells in RGD immune tissues than the one in REDV immune tissues. This observation implied the integrin ligand dependency of this *ex vivo* selection. Lastly, we examined whether antigen-specific antibodies can be produced using a non-transgenic WT mice as well (Fig. 5H). We observed 40% antigen-specific cells generated in the presence of soluble NP antigen and anti-FAS antibody (Fig. 5H). We also observed a simultaneous decrease in non-specific B cells upon anti-FAS addition, suggesting the immune tissues could potentially be used for developing antigen specific B cells using WT cells (Fig. 5H). We further noted the secretion of IgG1 NP-specific antibodies into the culture media with enzyme-linked immunosorbent assay (ELISA), which indicated that the enriched NP-specific GC-like B cells could be directed to secrete class-switched anti-NP antibodies following *ex vivo* activation, enrichment, and differentiation in the tissue platform (Fig. 5I).

4. Conclusion

In summary, we have developed a designer synthetic immune tissue that modulates GC B cell activation and facilitates its enrichment based on antigen affinity. Our results establish the first *ex vivo* tissue-like platform that is capable of inducing selective enrichment of antigen-specific GC-like B cells. We note that the current tissue model only captures a limited set of signals found in lymphoid tissues and focus specifically in the GC area. Future work will focus on incorporating T cells, dendritic cells, macrophages, which are all critical for *in vivo* dynamics, either as cells or as functionalized signaling biomolecules [17,35], and expand the system towards organ-on-chip approaches [36] or functionalization of FAS-ligand [37]. Nevertheless, the work is an important new step towards developing a rather complex GC-like system with antigen-specific B cell immune response, where future engineering of advanced biomaterials could lead us and others to demonstrate B cell zonal migration, rare cell section process, and B cell affinity maturation using complex antigens. Here, we used a combination of a hapten antigen NP and B1-8^{hi} mouse model to provide proof-of-concept results, however NP requires a limited set of somatic mutations and future work will determine ability to perform antigen specificity with more complex antigens such as Zika, HIV, or influenza. We expect that *ex vivo* immune tissues could potentially facilitate timely development of effective vaccines against infectious diseases and cancers in the future, and enable discovery of new classes of immunogenic antigens. We also anticipate that such ex vivo immune tissues will facilitate studies in hematological malignancies, many of which arise in the germinal centers and involve epigenetic changes.

Data availability

All data analyzed during this study are included in this published article (and its supplementary information files). The raw data required to reproduce these findings are available from the corresponding author on reasonable request.

Contributions

Conceptualization, A.P. and A.S.; Methodology, A.P., S.B.S, and A.S.; Resources, W.B. and A.M.M.; Intellectual input, A.A;

Manuscript writing, A.P and A.S. wrote the manuscript and all authors provided comments; Funding Acquisition, A.S.

Acknowledgement

We acknowledge financial support from the National Institute of Allergy and Infectious Diseases of the National Institutes of Health (Grant Number: 1R01AI132738-01A1 awarded to A.S) and the National Science Foundation CAREER award (Grant Number: DMR-1554275 awarded to A.S). We acknowledge the Cornell University Biotechnology Resource Center (BRC) Imaging Facility and NIH 1S10RR025502 for data collected on the Zeiss LSM 710 Confocal. Opinions, interpretations, conclusions, and recommendations are those of the authors and are not endorsed by the funding agencies.

Appendix A. Supplementary data

Supplementary data related to this article can be found at https://doi.org/10.1016/j.biomaterials.2018.06.034.

References

[1] J.M. Tas, et al., Visualizing antibody affinity maturation in germinal centers, Science 351 (2016) 1048–1054.
[2] N.S. De Silva, U. Klein, Dynamics of B cells in germinal centres, Nat. Rev. Immunol. 15 (2015) 137–148.
[3] Z. Shulman, et al., T follicular helper cell dynamics in germinal centers, Science 341 (2013) 673–677.
[4] G.D. Victora, et al., Germinal center dynamics revealed by multiphoton microscopy with a photoactivatable fluorescent reporter, Cell 143 (2010) 592–605.
[5] L. Mesin, J. Ersching, G.D. Victora, Germinal center B cell dynamics, Immunity 45 (2016) 471–482.
[6] B. Schiemann, et al., An essential role for BAFF in the normal development of B cells through a BCMA-independent pathway, Science 293 (2001) 2111–2114.
[7] B.A. Heesters, R.C. Myers, M.C. Carroll, Follicular dendritic cells: dynamic antigen libraries, Nat. Rev. Immunol. 14 (2014) 495–504.
[8] X. Wang, L.B. Rodda, O. Bannard, J.G. Cyster, Integrin-mediated interactions between B cells and follicular dendritic cells influence germinal center B cell fitness, J. Immunol. 192 (2014) 4601–4609.
[10] S.L. Nutt, P.D. Hodgkin, D.M. Tarlinton, L.M. Corcoran, The generation of antibody-secreting plasma cells, Nat. Rev. Immunol. 15 (2015) 160–171.
[11] A. Purwada, S.B. Shah, W. Beguelin, A. Melnick, A. Singh, Modular immune organoids with integrin ligand specificity differentially regulate Ex vivo B Cell activation, ACS Biomater. Sci. Eng. 3 (2017) 214–225.
[12] G. Koopman, et al., Adhesion through the LFA-1 (CD11a/CD18)-ICAM-1 (CD54) and the VLA-4 (CD49d)-VCAM-1 (CD106) pathways prevents apoptosis of germinal center B cells, J. Immunol. 152 (1994) 3760–3767.
[13] Y.R. Carrasco, F.D. Batista, B-cell activation by membrane-bound antigens is facilitated by the interaction of VLA-4 with VCAM-1, EMBO J. 25 (2006) 889–899.
[14] W. Beguelin, et al., EZH2 enables germinal centre formation through epigenetic silencing of CDKN1A and an Rb-E2F1 feedback loop, Nat. Commun. 8 (2017) 877.
[15] A. Purwada, et al., Ex vivo engineered immune organoids for controlled germinal center reactions, Biomaterials 63 (2015) 24–34.
[16] A. Purwada, A. Singh, Immuno-engineered organoids for regulating the Kinetics of B cell development and antibody production, Nat. Protoc. 12 (2017) 168–182.
[17] E.A. Gosselin, H.B. Eppler, J.S. Bromberg, C.M. Jewell, Designing natural and synthetic immune tissues, Nat. Mater. 17 (2018) 484–498.
[18] T. Nojima, et al., In-vitro derived germinal centre B cells differentially generate memory B or plasma cells in vivo, Nat. Commun. 2 (2011) 465.
[19] E.A. Phelps, et al., Maleimide cross-linked bioactive PEG hydrogel exhibits improved reaction kinetics and cross-linking for cell encapsulation and in situ delivery, Adv. Mater. 24 (2012) 64–70, 62.
[20] R. Cruz-Acuna, et al., Synthetic hydrogels for human intestinal organoid generation and colonic wound repair, Nat. Cell Biol. 19 (2017) 1326–1335.
[21] T.T. Lee, et al., Light-triggered in vivo activation of adhesive peptides regulates cell adhesion, inflammation and vascularization of biomaterials, Nat. Mater. 14 (2015) 352–360.
[22] W. Béguelin, et al., EZH2 is required for germinal center formation and somatic EZH2 mutations promote lymphoid transformation, Cancer Cell 23 (2013) 677–692.
[23] W. Beguelin, et al., EZH2 and BCL6 cooperate to assemble CBX8-BCOR complex to repress bivalent promoters, mediate germinal center formation and lymphomagenesis, Cancer Cell 30 (2016) 197–213.
[24] M. Caganova, et al., Germinal center dysregulation by histone methyltransferase EZH2 promotes lymphomagenesis, J. Clin. Invest. 123 (2013) 5009–5022.
[25] T. Kurosaki, M. Kurosaki, Transphosphorylation of Bruton's tyrosine kinase on tyrosine 551 is critical for B cell antigen receptor function, J. Biol. Chem. 272 (1997) 15595–15598.
[26] A.M. Khalil, J.C. Cambier, M.J. Shlomchik, B cell receptor signal transduction in the GC is short-circuited by high phosphatase activity, Science 336 (2012) 1178–1181.
[27] Y. Yamanashi, et al., Role of the rasGAP-associated docking protein p62 dok in negative regulation of B cell receptor-mediated signaling, Gene Dev. 14 (2000) 11–16.
[28] U. Klein, R. Dalla-Favera, Germinal centres: role in B-cell physiology and malignancy, Nat. Rev. Immunol. 8 (2008) 22–33.
[29] T. Fukuda, et al., Disruption of the Bcl6 gene results in an impaired germinal center formation, J. Exp. Med. 186 (1997) 439–448.
[30] H. Niu, H.Y. Bihui, R. Dalla-Favera, Antigen receptor signaling induces MAP kinase-mediated phosphorylation and degradation of the BCL-6 transcription factor, Gene Dev. 12 (1998) 1953–1961.
[31] G.D. Victora, et al., Identification of human germinal center light and dark zone cells and their relationship to human B-cell lymphomas, Blood 120 (2012) 2240–2248.
[32] J.C. Rathmell, et al., CD95 (Fas)-dependent elimination of self-reactive B cells upon interaction with CD4+ T cells, Nature 376 (1995) 181–184.
[33] T.A. Shih, M. Roederer, M.C. Nussenzweig, Role of antigen receptor affinity in T cell-independent antibody responses in vivo, Nat. Immunol. 3 (2002) 399–406.
[34] Y. Aiba, et al., Preferential localization of IgG memory B cells adjacent to contracted germinal centers, Proc. Natl. Acad. Sci. U. S. A. 107 (2010) 12192–12197.
[35] A. Singh, Biomaterials innovation for next generation ex vivo immune tissue engineering, Biomaterials 130 (2017) 104–110.
[36] F. Apoorva, et al., How biophysical forces regulate human B cell lymphomas, Cell Rep. 23 (2018) 499–511.
[37] D.M. Headen, et al., Local immunomodulation with Fas ligand-engineered biomaterials achieves allogeneic islet graft acceptance, Nat. Mater. (2018), https://doi.org/10.1038/s41563-018-0099-0.